Journal of Quantitative Spectroscopy & Radiative Transfer 149 (2014) 146–157

Contents lists available at ScienceDirect

Journal of Quantitative Spectroscopy & Radiative Transfer

journal homepage: www.elsevier.com/locate/jqsrt

# Lamb dip spectroscopy with the use of frequency-modulated radiation

Victor P. Kochanov [a,b,*], Sergey P. Belov [c], German Yu. Golubiatnikov [c]

[a] V.E. Zuev Institute of Atmospheric Optics, Siberian Branch, Russian Academy of Sciences, 1 Academician Zuev Square, 634021 Tomsk, Russia
[b] Tomsk State University, Tomsk 634050 Russia
[c] Institute of Applied Physics of the Russian Academy of Sciences, 46 Uljanova St., 603950 Nizhniy Novgorod, Russia

ARTICLE INFO

*Article history:*
Received 5 June 2014
Received in revised form
16 July 2014
Accepted 16 August 2014
Available online 23 August 2014

*Keywords:*
Lamb dip
Frequency modulation
Harmonics
Line profiles

ABSTRACT

A theory for molecular nonlinear absorption resonance in a standing electromagnetic wave recorded with the use of frequency-modulated radiation is developed. Spectral line profiles for the second harmonic of modulation frequency derived for different actual cases have been tested by comparison with the experimental ones recorded for absorption lines of OCS and CO molecules in the mm-wave region. The derived line profiles describe all the qualitative features of the experimentally observed spectra including the apparent splitting of a nonlinear resonance at high modulation frequency and allow retrieving quantitative data on the collision line broadening coefficients.



## 1. Introduction

Hyperfine structure of many molecular transitions cannot be resolved by means of linear spectroscopy, the resolution of which is limited by Doppler line broadening. This problem of a great importance can be solved with the aid of nonlinear spectroscopy of saturated absorption whose resolution is higher by one to two orders of magnitude. But at present, methods of nonlinear spectroscopy [1], in spite of their evident advantage in resolution, have no widespread occurrence in quantitative molecular spectroscopy (e.g., one of the applications is reported in Ref. [2]). This is explained by a rather complex physics involved in nonlinear resonance forming that requires a thorough instrumental theory and a specific experimental technique. Consequently, the shape of nonlinear resonances differs to some extent from the collision-broadened Lorentzian line profile due to the action of the power line broadening [3], the transient flight effect [4,5], and the diffraction scattering of molecules, which causes a nonlinear dependence of the resonance width on gas pressure [6–8]. All these factors must be taken into account for the purpose of retrieving reliable data on pressure broadening and shifting coefficients from the recorded nonlinear absorption spectra.

In this paper, we consider historically the first method of nonlinear spectroscopy: nonlinear absorption resonance in contra-directional modes, which in the particular case of a standing wave is merely the Lamb dip [9,10]. The realization of this method in the mm- and sub-mm-wave regions with the use of an outer absorbing cell was performed earlier in the department of microwave spectroscopy of the Institute of Applied Physics of the Russian Academy of Sciences [11]. The goal is to develop the instrumental theory for this method, which is applicable to retrieving quantitative data on collision line widths and to test it experimentally.

The contrast of the narrow Lamb dip on the background of a Doppler-broadened spectral line typically does not exceed a few percent, and in order to increase the contrast, the frequency (or phase) modulation technique (FM) is used [11], the same as in linear spectroscopy [12–22]. Below we will consider primarily a Lamb dip detection at

* Corresponding author at: V.E. Zuev Institute of Atmospheric Optics, Siberian Branch, Russian Academy of Sciences, 1 Academician Zuev Square, 634021 Tomsk, Russia Fax: +7 3822 492086.
*E-mail address:* koch@iao.ru (V.P. Kochanov).

http://dx.doi.org/10.1016/j.jqsrt.2014.08.005
0022-4073/

the second harmonic of the modulation frequency. As is known [13–16], maximal amplitudes of the recorded harmonics increase with the increase of a modulation index (the ratio of the frequency deviation to the modulation frequency) up to a certain value of the latter. At the same time, the number of sidebands (harmonics) in FM radiation also increases with increasing of the modulation index. As a result, a second-harmonic line shape can be quite different from the second derivative of the Lamb dip on a frequency, which is a good approximation in the limit of small modulation indices [12]. This mechanism of a line shape distortion is one of most essential, and we take it into account in the instrumental theory in the first place.

Let us estimate the contributions to the width of the Lamb dip caused by physical effects supplemental to the collision line broadening listed above. In conditions of the experiment [11] carried out with the OCS molecule, the influence of the transient flight effect can be estimated with the use of the formula [5] $\gamma=\Gamma+0.58/\tau$, where $\gamma$ is the effective half-width, $\Gamma$ is the collision half-width, and $\tau=a/\bar{v}$ is the flight time of an active molecule across the light beam; $a$ is the beam's radius, and $\bar{v}$ is the most probable thermal speed of the molecule. This formula is valid in the range $0.5\le\Gamma\tau\le 2$ that corresponds to the range of gas pressure $0.4\ \text{mTorr}\le p\le 1.7\ \text{mTorr}$ at $a=5$ cm, $\bar{v}=286$ m/s, and $\Gamma/p\sim 6-7$ MHz/Torr. The part of $\gamma$ independent of pressure is $0.58/\tau=3.3$ kHz, and it reveals itself as a half-width at zero pressure when extrapolating the dependence $\Gamma(p)$ by a straight line. Thus, within the exploited pressure range, it is expedient to take into account the flight effect in the simplified manner on the stage of interpretation of the obtained data on the pressure line broadening.

The saturation effect can be estimated with the aid of the simple expression for power-broadened half-width [1,3] $\gamma=\Gamma(1+\kappa)^{1/2}$, where $\kappa$ is the saturation parameter equal to the ratio of radiation intensity to the intensity of absorption saturation. Since the depth of the Lamb dip is proportional to $\kappa$, and its typical value is a few percent, the contribution of the saturation effect to $\gamma$ is small enough and it can be easily controlled. Further theory will be constructed in the conventional approach where all the expressions for a line profile contain only the first nonlinear terms proportional to $\kappa$.

The dependence $\gamma$ $(p)$ becomes nonlinear due to the diffraction scattering of molecules at $\Gamma<\Gamma_d\equiv k\bar{v}\theta_d$ [6–8], where $k$ is the wave number and $\theta_d$ is the mean angle of the diffraction scattering. The diffraction angle can be estimated as $\theta_d\sim\lambda_{dB}/\rho_W=\hbar/(\mu\bar{v}\rho_W)$ [8], where $\lambda_{dB}$ is the de Broglie wave length, $\rho_W$ is the Weisskopf radius, and $\mu$ is the reduced mass of colliding molecules. For the 424.78 GHz OCS spectral line, $k\bar{v}=405.8$ kHz, and from the above formulas follow $\theta_d=3.7$ mrad and $\Gamma_d=1.5$ kHz. From the latter estimated value and pressure broadening coefficient taken above, $\Gamma/p$ ~7 MHz/Torr, it follows that the diffraction scattering is pronounced at pressures below 0.2 mTorr. More detailed investigation of this effect is carried out in Section 2.

## 2. Lamb dip without modulation of radiation

The detailed theory of a nonlinear behavior of the nonlinear resonance width as a function of gas pressure was developed in Ref. [8] in the case of a running wave. In this section, we generalize it to the case of a standing wave with the electrical component represented as

$$E(t,z)=2E\ \cos(\omega t)\cos(kz), \tag{1}$$

where $E$ is the field amplitude that is constant in the considered optically thin medium, $\omega$ and $k$ are the frequency and the wave number of radiation, respectively.

The density matrix equations for a two-level quantum system with account of the diffraction scattering are [8]

$$\left(\frac{\partial}{\partial t}+v\frac{\partial}{\partial z}+\nu\right)n-\int_{-\infty}^{\infty}A(v-v_1)n(v_1)dv_1=\gamma W_M(v)n_0+\frac{4dE}{\hbar}\mathrm{Re}(i\rho),$$

$$\left(\frac{\partial}{\partial t}+v\frac{\partial}{\partial z}+\nu+i\omega_0\right)\rho-\int_{-\infty}^{\infty}A(v-v_1)\rho(v_1)dv_1=\frac{idE}{\hbar}n;$$

$$A(v-v_1)=\frac{\nu_d}{2\Delta_d}\exp\left(-\frac{|v-v_1|}{\Delta_d}\right),\ W_M(v)=\frac{1}{\sqrt{\pi}\bar{v}}\exp\left(-\frac{v^2}{\bar{v}^2}\right),$$

$$n_0=\int_{-\infty}^{\infty}n(v)dv,\ \gamma=\nu-\nu_d,\ \bar{v}=\sqrt{2k_BT/m}. \tag{2}$$

Here $\rho$ is the off-diagonal matrix element of the density matrix or, with the accuracy to a factor, the polarization of an active molecule; $n$ is the population difference; $v_1$ and $v$ are molecular velocity projections onto the wave vector before and after collision, respectively; $d$ is the matrix element of a dipole moment at the actual transition with the eigenfrequency $\omega_0$; $\nu$ and $\nu_d$ are the output and input collision integral frequencies [8,23,24], respectively; $A$ is the diffraction part of the collision integral kernel[1] [23]; $\Delta_d\sim\theta_d\bar{v}$ [23,25] is the half-width at the $1/e$ height of the kernel; $k_B$ is the Boltzmann constant; $\hbar$ is the Plank constant; $T$ is the gas temperature, and $m$ is the mass of an absorbing molecule. Furthermore, the dependence of the collision relaxation constants on molecular speed does not play a major role, and hence it is disregarded.

By putting

$$\rho=(R_+e^{ikz}+R_-e^{-ikz})e^{-i\omega t},\ n=\underset{t,z}{\mathrm{const}} \tag{3}$$

and using the rotating wave approximation, we obtain from Eq. (2) the stationary equations

$$\nu n(v)-\frac{\nu_d}{2\Delta_d}\int_{-\infty}^{\infty}\exp(-|v-v_1|/\Delta_d)n(v_1)dv_1 + 4V\left[R''_+(v)+R''_-(v)\right]=\frac{n_0\gamma}{\sqrt{\pi}\bar{v}}\exp(-v^2/\bar{v}^2),$$

$$\left[\nu-i(\Omega-kv)\right]R_+(v)-\frac{\nu_d}{2\Delta_d}\int_{-\infty}^{\infty}\exp(-|v-v_1|/\Delta_d)R_+(v_1)dv_1=iVn(v),$$

$$\left[\nu-i(\Omega+kv)\right]R_-(v)-\frac{\nu_d}{2\Delta_d}\int_{-\infty}^{\infty}\exp(-|v-v_1|/\Delta_d)R_-(v_1)dv_1=iVn(v);$$

$$V=\frac{dE}{2\hbar},\ \Omega=\omega-\omega_0,\ R_\pm=R'_\pm+iR''_\pm. \tag{4}$$

The absorption coefficient is defined from the wave equation for slow field amplitude as

$$K(\Omega)=\frac{8\pi Nd\omega}{cE}\int_{-\infty}^{\infty}R''_+(v)dv, \tag{5}$$

[1] Hard velocity-changing collisions are omitted, since they lead to irrelevant distortion (collision line narrowing [26]) of the Doppler-broadened pedestal for narrow nonlinear absorption spectrum.

where $N$ is the density of absorbing molecules and $c$ is the light speed.

The solution of Eqs. (4) and (5) can be obtained under supposition of a weak nonlinearity by means of Fourier transformation and it reads

$$K(\Omega)=\frac{S\gamma}{2\pi^{3/2}\nu k\bar{v}}\left\{\int_0^\infty ds\frac{\exp\left[-s^2/4-\tilde{\nu}s+\frac{\tilde{\nu}_d}{\theta_d}tan^{-1}(\theta_d s)\right]\cos(\tilde{\Omega}s)}{1-\xi/(1+\theta_d^2 s^2)}-\right.$$
$$4\kappa\tilde{\nu}\int_0^\infty ds\frac{\exp\left[-s^2/4-\tilde{\nu}s+\frac{\tilde{\nu}_d}{\theta_d}tan^{-1}(\theta_d s)\right]\cos(\tilde{\Omega}s)}{1-\xi/\left(1+\theta_d^2 s^2\right)}$$
$$\int_0^\infty ds_1\exp(-s_1^2/4-\tilde{\nu}s_1)\cos(\tilde{\Omega}s_1)$$
$$\times\left[\frac{\exp\left(ss_1/2+\frac{\tilde{\nu}_d}{\theta_d}tan^{-1}\left(\frac{\theta_d s_1}{1-\theta_d^2 s(s_1-s)}\right)\right)}{1-\xi/(1+\theta_d^2(s_1-s)^2)}\right.$$
$$\left.\left.+\frac{\exp\left(-ss_1/2+\frac{\tilde{\nu}_d}{\theta_d}tan^{-1}\left(\frac{\theta_d s_1}{1+\theta_d^2 s(s_1+s)}\right)\right)}{1-\xi/(1+\theta_d^2(s_1+s)^2)}\right]\right\};$$
$$S=\frac{8\pi^2 N n_0 d^2\omega}{c\hbar},\quad \kappa=\frac{V^2}{\nu^2},\quad \xi=\frac{\nu_d}{\nu},\quad \tilde{\nu}=\frac{\nu}{k\bar{v}},$$
$$\tilde{\nu}_d=\frac{\nu_d}{k\bar{v}},\quad \tilde{\Omega}=\frac{\Omega}{k\bar{v}}. \tag{6}$$

If we neglect the diffraction scattering, then $\nu_d$, $\xi\to 0$ and $\nu\to\gamma$. In this limiting case, we obtain from Eq. (6)

$$K(\Omega)=\frac{S}{\sqrt{\pi}k\bar{v}}\mathrm{Re}\left\{w(\tilde{\Omega}+i\tilde{\gamma})-\kappa\tilde{\gamma}\left[\frac{4}{\sqrt{\pi}}-4\left(\tilde{\gamma}-i\tilde{\Omega}\right)w\left(\tilde{\Omega}+i\tilde{\gamma}\right)+\right.\right.$$
$$\left.\left.\left(\frac{1}{\tilde{\gamma}}+\frac{2}{\tilde{\gamma}-i\tilde{\Omega}}-\frac{i}{\tilde{\Omega}}\right)w(\tilde{\Omega}+i\tilde{\gamma})+\left(\frac{1}{\tilde{\gamma}}+\frac{i}{\tilde{\Omega}}\right)w(-\tilde{\Omega}+i\tilde{\gamma})\right]\right\};$$
$$w(z)=e^{-z^2}\mathrm{erfc}(-iz),\ \mathrm{erfc}(z)=\frac{2}{\sqrt{\pi}}\int_z^\infty e^{-t^2}dt,\ \tilde{\gamma}=\frac{\gamma}{k\bar{v}}, \tag{7}$$

where $\mathrm{erfc}(z)$ is the complementary error function of a complex argument [27].

The simple approximation for $K(\Omega)$ in Eq. (7) based on an expansion of the $w(z)$ function at $\gamma/(k\bar{v})<0.2$ and $\kappa<0.3$ is

$$K_a(\Omega)=\frac{S}{\sqrt{\pi}k\bar{v}}\left[\!\left[e^{-\tilde{\Omega}^2}-\kappa\left\{\frac{1}{2}\left(1+\frac{1}{1+\Omega^2/\gamma^2}\right)\right.\right.\right.$$
$$\left.\left.\left.e^{-\tilde{\Omega}^2}+\frac{\tilde{\gamma}}{\sqrt{\pi}}+\frac{\tilde{\gamma}}{\sqrt{\pi}}\left(\frac{1}{1+\Omega^2/\gamma^2}-2\tilde{\Omega}^2\right)e^{-2\tilde{\Omega}^2/3}\right\}\right]\!\right]$$
$$\times[1+(1+0.42\kappa)\tilde{\gamma}]^{-1}. \tag{8}$$

Least squares fitting of $K_a(\Omega)$ in Eq. (8) to the line profile $K(\Omega)$ in Eq. (6) calculated at $\xi=0.5$, $\theta_d=0.05$, and $\kappa=0.2$ gives the nonlinear dependence of the retrieved effective half-width $\gamma_{eff}$ on the collision half-width $\gamma=\nu-\nu_d$ that was used in calculations of the line profile Eq. (6) derived with account of the diffraction scattering (Fig. 1). The slopes $d\gamma_{eff}/d\gamma$ at minimal and maximal values of $\gamma$ that are respectively represented by straight lines 1 and 2 in Fig. 1 differ by 45%. The point of crossing of the slopes is $\gamma_0=0.041k\bar{v}\propto\theta_d$ and it demarcates the regions of a gas pressure where the diffraction scattering is essential, or not. In conditions of the measurements [11], $\gamma_0$ corresponds to the pressure $p_0=0.18$ mTorr, which coincides with the estimation made in Section 1. Hence, at higher pressures,

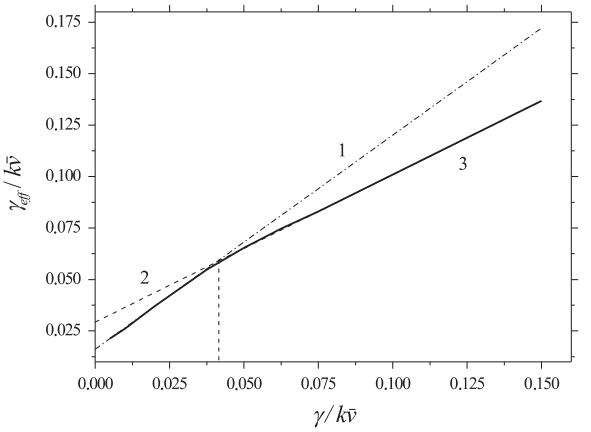


**Fig. 1.** Nonlinear dependence of the effective Lamb dip half-width $\gamma_{eff}$ on the homogeneous collision half-width $\gamma$ proportional to a gas pressure (curve 3). The straight line 1 is determined by the expression $\gamma_{eff}=1.04\gamma+0.016\ k\bar{v}$ and it gives the slope at low pressures. The expression for the straight line 2 representing the slope at high pressures is $\gamma_{eff}=0.72\gamma+0.029k\bar{v}$. The vertical line at $\gamma=0.0415k\bar{v}$ demarcates the regions of "low" and "high" pressures.

$p>0.7$ mTorr, the diffraction scattering does not noticeably change the linear dependence of the observable collision half-width on pressure. The consequences of the effect under consideration consist in the diminishing the pressure broadening coefficient retrieved by means of Eq. (8) by a few percent and the appearance of nonzero residual, $\gamma<0.025k\bar{v}$, at $p\to 0$. Taking these circumstances into account, in further theory we will disregard the influence of the diffraction scattering because the exploited range of pressures is higher than 0.2 mTorr [11]. This allows one to use simpler expressions for a line profile. In particular, in the case of a small modulation index, the first or second derivatives of the line profile $K_a(\Omega)$ in Eq. (8) can be used in data processing.

## 3. Arbitrary modulation index and frequency

The FM radiation at the input ($z=L$) of the absorbing cell can be written as the sum of harmonics [12,27]

$$E_-(L,t)=E\cos[\omega t+\delta\sin(\nu t)]=E\sum_{n=-\infty}^{\infty}J_n(\delta)\cos[(\omega+n\nu)t], \tag{9}$$

where $L$ is the length of the absorbing medium, $\nu$ and $\delta$ are the frequency and the index of modulation, respectively, and $J_n$ is the Bessel function [27].

Nonlinear resonances are recorded at low gas pressures. If the optical thickness of an absorbing medium is small enough, then the phase shift of the radiation passing through the medium, which is caused by the absorption, is also small (it will be considered separately in Section 5). Hence, in the first approximation we can set the field inside an absorbing cell as a sum of two polyharmonical waves propagating in opposite directions:

$$E(z,t)=E\sum_{n=-\infty}^{\infty}\{E_n^-(z)\cos[(\omega+n\nu)t+k_n z]$$
$$+E_n^+(z)\cos[(\omega+n\nu)t-k_n z]\}. \tag{10}$$

Here $E_n^+$ and $E_n^-$ are real dimensionless electrical field amplitudes and $k_n \approx (\omega + n\nu)/c$ are the wavenumbers of harmonics. As a result of the accepted above assumption of small absorption, only cosines are presented in Eq. (10). In the case of noticeable radiation absorption, the field in the medium must also contain sines [see Eq. (24)].

In order to find the medium response (macroscopic polarization) we use Eq. (2) where $\nu \to \gamma$ and $\nu_d$, $A \to 0$. These replacements mean that the effect of the diffraction scattering is disregarded. Together with Eq. (2), we use the field of Eq. (10), and also the following representation of the field-induced polarization:

$$\rho(z,t) = \sum_{m=-\infty}^{\infty} [\![ R_m^-(z)\exp\{-i[(\omega+m\nu)t + k_m z]\} + R_m^+(z)\exp\{-i[(\omega+m\nu)t - k_m z]\} ]\!]. \quad (11)$$

The solution of Eqs. (2), (10), and (11) carried out in the rotating wave approximation after averaging over velocities is

$$\langle R_m^{\pm}(z)\rangle = \tfrac{1}{2Nd}\chi_m^{\pm} E_m^{\pm}(z),$$

$$\chi_m^{\pm} \approx \frac{2iNdVn_0}{\gamma}\frac{1}{\sqrt{\pi}}\int_{-\infty}^{\infty} dt \frac{\exp(-t^2)}{1 - i(\Omega_m \mp k_m\bar{v}t)/\gamma} \times\left\{1 - 4\kappa\sum_{n=-\infty}^{\infty}\left[\frac{(E_n^-)^2}{1+(\Omega_n + k_n\bar{v}t)^2/\gamma^2} + \frac{(E_n^+)^2}{1+(\Omega_n - k_n\bar{v}t)^2/\gamma^2}\right]\right\};$$

$$\kappa = V^2/\gamma^2, \Omega_m = \Omega + m\nu, \chi_m^{\pm} = \chi_m^{\pm\prime} + i\chi_m^{\pm\prime\prime},$$

$$\langle R\rangle = \int_{-\infty}^{\infty} R(v)dv, \quad (12)$$

where $\chi^{\pm}$ are complex susceptibilities for two radiation waves including parts that are linear and nonlinear on the field's amplitude.

The macroscopic medium polarization related to the radiation absorption taking into account Eqs. (11) and (12) is

$$P = 2Nd\mathrm{Re}\rho = \sum_{m=-\infty}^{\infty}[\chi_m^{-\prime\prime}\sin\Psi_m^- + \chi_m^{+\prime\prime}\sin\Psi_m^+];$$

$$\Psi_m^{\pm} = (\omega + m\nu)t \mp k_m z. \quad (13)$$

The wave equations for slow field amplitudes obtained with the use of Eq. (13) in the approximation of $|m|\nu \ll \omega$ are

$$2\frac{dE_m^+}{dz} \approx -\frac{4\pi\omega}{c}\chi_m^{+\prime\prime}E_m^+,$$

$$2\frac{dE_m^-}{dz} \approx \frac{4\pi\omega}{c}\chi_m^{-\prime\prime}E_m^-. \quad (14)$$

After concretizing susceptibilities Eq. (12) and performing a transformation from the coordinate $z$ to the dimensionless optical thickness $\zeta$, Eq. (14) takes the form

$$\frac{dE_m^+}{d\zeta} = -\tfrac{1}{2}FE_m^+, \quad \frac{dE_m^-}{d\zeta} = \tfrac{1}{2}FE_m^-,$$

$$F = f_{0m} - 4\kappa\sum_{n=-\infty}^{\infty}(f_{1mn}^+ E_n^{+2} + f_{2mn}^+ E_n^{-2}),$$

$$f_{0m} = \frac{k\bar{v}}{\pi^{3/2}\gamma}\int_{-\infty}^{\infty} dt\frac{\exp(-t^2)}{1+(\Omega_m \mp k\bar{v}t)^2/\gamma^2},$$

$$f_{1mn}^{\pm} = \frac{k\bar{v}}{\pi^{3/2}\gamma}\int_{-\infty}^{\infty} dt\frac{\exp(-t^2)}{\left[1+(\Omega_m \mp k\bar{v}t)^2/\gamma^2\right]\left[1+(\Omega_n - k\bar{v}t)^2/\gamma^2\right]},$$

$$f_{2mn}^{\pm} = \frac{k\bar{v}}{\pi^{3/2}\gamma}\int_{-\infty}^{\infty} dt\frac{\exp(-t^2)}{\left[1+(\Omega_m \mp k\bar{v}t)^2/\gamma^2\right]\left[1+(\Omega_n + kvt)^2/\gamma^2\right]},$$

$$\zeta = Qz,\ Q = \frac{4\pi^2 Nn_0 d^2\omega}{c\hbar k\bar{v}},\ \zeta_L = QL,\ k \cong \frac{\omega}{c};$$

$$E_m^-(\zeta_L) = J_m(\delta),\ E_m^+(0) = -\sqrt{q}E_m^-(0), \quad (15)$$

where $q$ is the reflection coefficient and the boundary conditions are written in the last line.

The changing of variables in Eq. (15)

$$E_m^+ = \tilde{E}_m^+\exp(-f_{0m}\zeta/2),\ E_m^- = \tilde{E}_m^-\exp[-f_{0m}(\zeta_L - \zeta)/2] \quad (16)$$

allows one to handle the small nonlinear part of absorption separately:

$$\frac{d\tilde{E}_m^+}{d\zeta} = 2\kappa G_+\tilde{E}_m^+, \frac{d\tilde{E}_m^-}{d\zeta} = -2\kappa G_-\tilde{E}_m^-,$$

$$G_{\pm} = \sum_{n=-\infty}^{\infty}\{f_{1mn}^{\pm}\exp(-f_{0n}\zeta)(E_n^+)^2 + f_{2mn}^{\pm}\exp[-f_{0n}(\zeta_L - \zeta)](E_n^-)^2\}. \quad (17)$$

The solution of Eq. (17) in the approximation of $\kappa \ll 1$ after performing the integration in coefficients $f$ (Eq. (15)) leads to the following expression for the field amplitude of the $m$th sideband of radiation passed through the absorbing cell:

$$E_m^+(\zeta_L) = -\sqrt{q}\exp(-f_{0m}\zeta_L)J_m(\delta)\left\{1 + \kappa\zeta_L\sum_{n=-\infty}^{\infty}J_n^2(\delta)A_{m,n}\right\},$$

$$A_{m,n} = (1 + e^{-f_{0n}\zeta_L})(1 + qe^{-f_{0n}\zeta_L})F_{mn},$$

$$F_{mn} = \frac{1}{2\sqrt{\pi}}\mathrm{Re}\left\{\left[\frac{1}{2 - i(\Omega_m - \Omega_n)/\gamma} + \frac{1}{2 - i(\Omega_m + \Omega_n)/\gamma} - \frac{i\gamma}{\Omega_m - \Omega_n} - \frac{i\gamma}{\Omega_m + \Omega_n}\right]w\left(\frac{\Omega_m + i\gamma}{k\bar{v}}\right) + \left[\frac{1}{2 - i(\Omega_m + \Omega_n)/\gamma} + \frac{i\gamma}{\Omega_m - \Omega_n}\right]w\left(\frac{\Omega_n + i\gamma}{k\bar{v}}\right) + \left[\frac{1}{2 - i(\Omega_m - \Omega_n)/\gamma} + \frac{i\gamma}{\Omega_m + \Omega_n}\right]w\left(\frac{-\Omega_n + i\gamma}{k\bar{v}}\right)\right\},$$

$$f_{0m} = \frac{1}{\sqrt{\pi}}\mathrm{Re}w\left(\frac{\Omega_m + i\gamma}{k\bar{v}}\right). \quad (18)$$

The averaged over fast oscillations rectified signal from a detector at the frequency $l\nu$ for the harmonic with a number $l$ is the sought-for line profile that follows from Eqs. (10) and (18):

$$K_l(\Omega) \propto \langle E_{+(l)}^2\rangle \propto \sum_{m=-M+1}^{M-1} J_m(\delta)J_{m-l}(\delta)\exp[-(f_{0m} + f_{0m-l})\zeta_L] \times\left[1 + \kappa\zeta_L\sum_{n=-M+1}^{M-1}J_n^2(\delta)(A_{m,n} + A_{m,n-l})\right], \quad (19)$$

where $E_+$ corresponds to the second term in Eq. (10) and the summing is restricted by number $M$ that is dependent on the modulation index $\delta$. Numerical calculations show that the line profile in Eq. (19) can be found with the inaccuracy of $10^{-4}$ by setting $M = [1.8\delta + 3.4]$, where brackets denote an integer part of the evaluated expression inside them.

The expansion of the functions in Eqs. (18) and (19) into series in the small ratio $\gamma/(k\bar{v}) \ll 1$ gives

$$K_l(\Omega) \propto \sum_{m=-M+1}^{M-1} J_m(\delta)J_{m-l}(\delta)\exp[-(e^{-\tilde{\Omega}_m^2} + e^{-\tilde{\Omega}_{m-l}^2})\zeta_L/\sqrt{\pi}]$$

$$\times\left[1+\kappa\zeta_L\sum_{n=-M+1}^{M-1}J_n^2(\delta)(A_{m,n}+A_{m,n-l})\right],$$

$$A_{m,n}=\left[1+\exp\left(-e^{-\tilde{\Omega}_n^2}\zeta_L/\sqrt{\pi}\right)\right]\left[1+q\exp\left(-e^{-\tilde{\Omega}_n^2}\zeta_L/\sqrt{\pi}\right)\right]F_{mn},$$

$$\begin{aligned}F_{mn}=\frac{1}{2\sqrt{\pi}}\mathrm{Re}\Bigg\{&\left[\frac{1}{2-i(\Omega_m-\Omega_n)/\gamma}+\frac{1}{2-i(\Omega_m+\Omega_n)/\gamma}-\frac{i\gamma}{\Omega_m-\Omega_n}-\frac{i\gamma}{\Omega_m+\Omega_n}\right]\\&\times\left[e^{-\tilde{\Omega}_m^2}+\frac{2i}{\sqrt{\pi}}F(\tilde{\Omega}_m)\right]\\&+\left[\frac{1}{2-i(\Omega_m-\Omega_n)/\gamma}+\frac{1}{2-i(\Omega_m+\Omega_n)/\gamma}+\frac{i\gamma}{\Omega_m-\Omega_n}+\frac{i\gamma}{\Omega_m+\Omega_n}\right]e^{-\tilde{\Omega}_n^2}\\&+\frac{2i}{\sqrt{\pi}}\left[-\frac{1}{2-i(\Omega_m-\Omega_n)/\gamma}+\frac{1}{2-i(\Omega_m+\Omega_n)/\gamma}+\frac{i\gamma}{\Omega_m-\Omega_n}-\frac{i\gamma}{\Omega_m+\Omega_n}\right]F(\tilde{\Omega}_n)\Bigg\};\end{aligned}$$

$$F(x)=e^{-x^2}\int_0^x e^{-t^2}dt\underset{x<0.5}{\rightarrow}xe^{-2x^2/3},\ \tilde{\Omega}_m=\frac{\Omega_m}{k\bar{v}}. \qquad (20)$$

Here $F(x)$ is the Dawson function [27].

In order to eliminate the indeterminacies in the function $F_{mn}$ in Eq. (20), the following relationships have been used in numerical evaluation of the line profiles $K_l(\Omega)$:

$$\begin{aligned}&\frac{\gamma}{\nu(m-n)}\left[F(\tilde{\Omega}_m-\tilde{\Omega}_n)\right]\rightarrow_{n\rightarrow m}\frac{\gamma}{k\bar{v}}\left[1-2\tilde{\Omega}_mF(\tilde{\Omega}_m)\right],\\&\frac{\gamma}{2\Omega+(m+n)\nu}\left[F(\tilde{\Omega}_m)+F(\tilde{\Omega}_n)\right]\rightarrow_{\Omega\rightarrow-(m+n)\nu/2}\frac{\gamma}{2(m+n)\nu}\\&\left[F\frac{3m+n}{2}\tilde{v}+F\frac{m+3n}{2}\tilde{v}\right]\rightarrow_{n\rightarrow-m}\frac{\gamma}{k\bar{v}}\left[1-2m\nu F(m\tilde{v})\right].\end{aligned} \qquad (21)$$

The dependence of the second harmonic line profile $K_2(\Omega)$ in Eq. (20) on the modulation index $\delta$ is presented in Fig. 2. From the values of rescaling coefficients $b$ in Fig. 2, it is evident that the recorded signal significantly increases with the increase in $\delta$. At the same time, this gain attains by substantial increase in a calculation time due to the quadratic expansion of twofold summation in Eq. (20). Therefore, modulation indices optimal for data processing are $\delta\sim1-5$. The increase in the saturation parameter $\kappa$ does not essentially influence the maximal amplitude of the signal but it leads to the increase in the contrast of the nonlinear resonance (Fig. 3). As is seen from Fig. 4, when the modulation frequency $\nu$ exceeds the collision half-width $\gamma$, the narrow resonance splits. The amplitude of the resonance enlarges with the increase in $\nu$. The shapes of the line profile $K_l(\Omega)$ Eq. (20) for harmonics with $l=0-3$ are shown in Fig. 5. The recorded signal substantially decreases for higher harmonics with a simultaneous increase in the contrast of a nonlinear resonance.

## 4. Low modulation frequency

Since the expression for the line profile in Eq. (12) is complicated enough, there is a need to derive a simpler one. It is possible to do this in the case of a low modulation frequency with the aid of an adiabatic approach such as was used in Refs. [14,15]. As is seen from Eq. (8), the

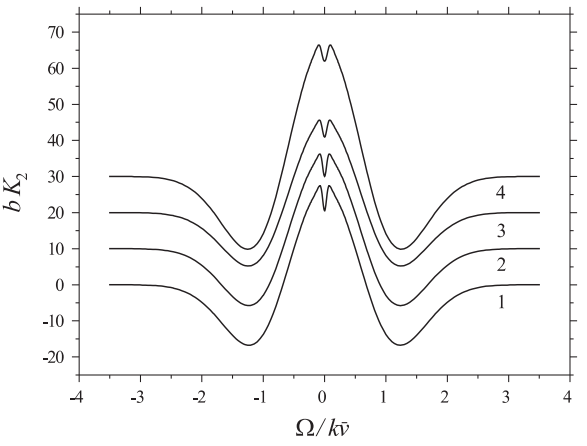


**Fig. 2.** The line profiles $K_2(\Omega)$ Eq. (20) for the second FM harmonic at different modulation indices $\delta=0.5$ (curve 1), 1 (2), 2 (3), and 3 (4); $b=28.89$ (curve 1), 6.84 (2), 1.63 (3), and 1 (4); $\gamma=0.075k\bar{v}$, $\nu=0.025k\bar{v}$, $\kappa=0.01$, $\zeta=0.15$, and $q=1$. Zero levels for curves 2–4 are shifted on the value $10\times(n-1)$, where $n$ is the number of the curve.

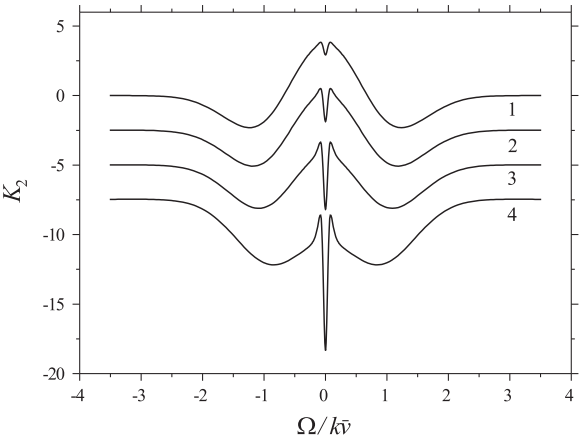


**Fig. 3.** The line profiles $K_2(\Omega)$ Eq. (20) at different saturation parameters $\kappa=0.01$ (curve 1), 0.025 (2), 0.05 (3), and 0.1 (4); $\delta=1$, $\gamma=0.075k\bar{v}$, $\nu=0.025k\bar{v}$, $\zeta=0.15$, and $q=1$. Zero levels for curves 2–4 are displaced for the sake of clarity.

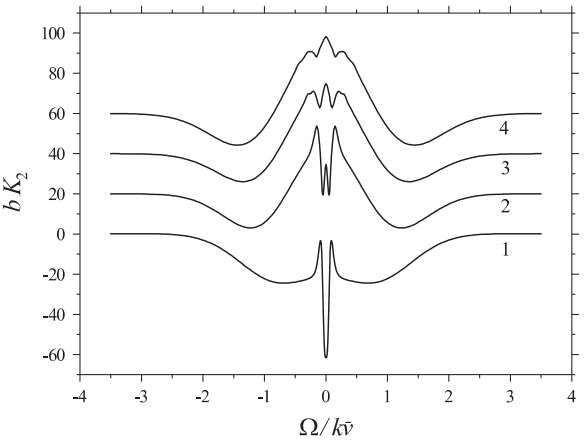


**Fig. 4.** Splitting of nonlinear resonance $K_2(\Omega)$ Eq. (20) at different modulation frequencies $\nu/k\bar{v}=0.05$ (curve 1), 0.1 (2), 0.2 (3), and 0.3 (4); $\gamma=0.05k\bar{v}$, $\delta=1$, $\kappa=0.2$, $\zeta=0.15$, and $q=1$; $b=1$ (curve 1), 0.45 (2), 0.119 (3), and 0.07 (4); zero levels for curves 2–4 are displaced.

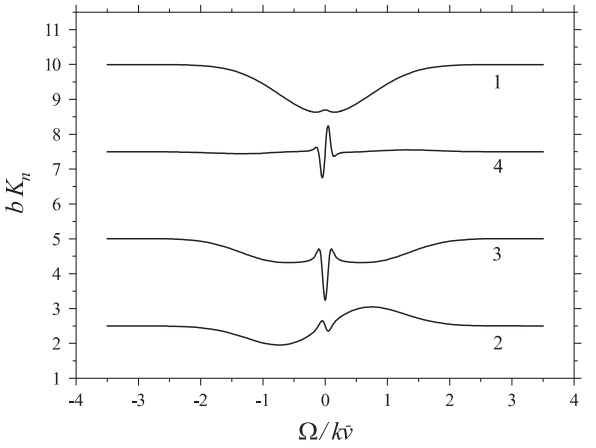


**Fig. 5.** Lamb dip line shapes for the different FM harmonics $K_n(\Omega)$ Eq. (20) for $n=0$ (curve 1), 1 (2), 2 (3), and 3 (4); $\delta=2$, $\gamma=0.075k\bar{v}$, $\nu=0.03k\bar{v}$, $\kappa=0.2$, $\zeta=0.15$, and $q=1$; $b=1$ (curve 1), 14.5 (2), 367 (3), and 2750 (4); zero levels are displaced.

narrow Lamb dip is associated with the Lorentzian profile. This enables one to ignore the Doppler line broadening and to treat the nonlinear resonance as a homogeneously broadened Lorentzian line profile caused by the absorption of a running-wave radiation with a "frozen" modulation. The set of equations for this model is

$$\begin{aligned}
&\frac{d\rho}{dt}+(\gamma+i\omega_0)\rho=\frac{idn_0E}{\hbar};\\
&E=E\ \cos\ [\omega t+\delta\ \sin(\nu t)],\\
&\rho=R(t)\exp\{-i[\omega t+\delta\ \sin(\nu t)]\},\\
&\frac{dR}{dt}+\{\gamma-i[\Omega+\Delta\ \cos(\nu t)]\}R=\frac{idn_0E}{2\hbar},\Delta\equiv\delta\nu,\\
&K(\omega)=\frac{8\pi Nd\omega}{cE}R''(t),\\
&K(\Omega,t)=\frac{S}{\pi}\mathrm{Re}\frac{1}{\gamma-i[\Omega+\Delta\ \cos(\nu t)]}.
\end{aligned}\tag{22}$$

The second harmonic of $K(\Omega, t)$ Eq. (22) is proportional to

$$\int_{-\pi/2}^{\pi/2}\frac{\cos\ 2\tau}{\gamma-i(\Omega+\Delta\ \cos\ \tau)}d\tau$$

and gives the line profile

$$\begin{aligned}
K_2(\Omega)=\frac{S}{\pi}\mathrm{Re}\Big\{&1/\sqrt{\Delta^2+(\gamma+i\Omega)^2}\\
&-2/\left[\gamma+i\Omega+\sqrt{\Delta^2+(\gamma+i\Omega)^2}+\Delta^2/(\gamma+i\Omega)\right]\Big\}.
\end{aligned}\tag{23}$$

This formula,[2] with the addition of a quadratic polynomial as an approximation for the Doppler pedestal, can be used in a fast preliminary data processing in the case of $\nu<0.3\gamma$.

[2] Our attempt to compare Eq. (23) with the related formulas Eq. (13) in Ref. [15] and Eq. (27) in Ref. [14] failed because of an unfeasible spectral shape of the latter. At the same time, numerical evaluation of Eq. (26) [14] and Eq. (23) displays their coincidence though they have a different form. Thus, Eq. (13) [15] and Eq. (27) [14] contain an error caused by incorrect calculation of the real part in Eq. (26) [14].

## 5. Phase sensitive lock-in detection

The previous consideration presumes synchronous detection (or phase sensitive lock-in detection) of a certain harmonic of FM molecular absorption signal with the use of a single channel and square-law detector. A more elaborate experimental technique consists in dual channel detection with 90-degree phase shift between oscillations in the channels having the same frequency [16,18]. This method of registration allows recovering both the absorption and the dispersion components of the detected FM signal. Therefore, the radiation inside the medium must be treated in a complete form as

$$\begin{aligned}
E_{\pm}(z,t)=E\sum_n\{&E_{cn}^{\pm}(z)\cos\ [(\omega+n\nu)t\mp k_nz]\\
&+E_{sn}^{\pm}(z)\sin\ [(\omega+n\nu)t\mp k_nz]\}.
\end{aligned}\tag{24}$$

Here both the first and the second terms in braces are responsible for the absorption and the dispersion, as will be seen from Eqs. (26), (29), and (31) below.

Moreover, for the sake of simplicity, we will deal with the only wave of Eq. (24) that propagates in the positive direction, thus following the approach of Section 4 (except for the assumption of small $\nu$), and omit the indices "$\pm$". The input radiation is given by Eq. (9) as before.

For calculation of the medium polarization, we use Eq. (22) and set

$$\rho=\sum_m R_m\exp\{-i[(\omega+m\nu)t-k_mz]\}.\tag{25}$$

After substitution of Eqs. (24) and (25) into the first of Eq. (22), we have the solution

$$\begin{aligned}
&R_m=R'_m+iR''_m=\frac{idEn_0}{2\hbar}\frac{E_{cm}+iE_{sm}}{\gamma-i(\Omega+m\nu)};\\
&R''_m=\frac{dEn_0}{2\hbar}\frac{\gamma E_{cm}-(\Omega+m\nu)E_{sm}}{\gamma^2+(\Omega+m\nu)^2},\\
&R'_m=-\frac{dEn_0}{2\hbar}\frac{\gamma E_{sm}+(\Omega+m\nu)E_{cm}}{\gamma^2+(\Omega+m\nu)^2}.
\end{aligned}\tag{26}$$

From Eq. (26) we obtain the macroscopic polarization

$$\begin{aligned}
P=2Nd\mathrm{Re}\rho=2Nd\sum_m\{&R'_m\ \cos\ [(\omega+m\nu)t-k_mz]\\
&+R''_m\ \sin\ [(\omega+m\nu)t-k_mz]\}.
\end{aligned}\tag{27}$$

The use of Eqs. (24) and (27) also with the wave equation

$$\frac{\partial^2E}{\partial z^2}-\frac{1}{c^2}\frac{\partial^2E}{\partial t^2}=\frac{4\pi}{c^2}\frac{\partial^2P}{\partial t^2}\tag{28}$$

leads to the equations for slow amplitudes

$$\begin{aligned}
&2k_m\frac{dE_{cm}}{dz}-\left[k_m^2-\frac{(\omega+m\nu)^2}{c^2}\right]E_{sm}=-\frac{8\pi N(\omega+m\nu)^2}{c^2E}R''_m,\\
&2k_m\frac{dE_{sm}}{dz}+\left[k_m^2-\frac{(\omega+m\nu)^2}{c^2}\right]E_{cm}=\frac{8\pi N(\omega+m\nu)^2}{c^2E}R'_m.
\end{aligned}\tag{29}$$

After the definitions

$$\begin{aligned}
&k_m=\frac{\omega+m\nu}{c}\cong\frac{\omega}{c}\equiv k,\\
&\zeta\equiv\tilde{Q}z,\quad\tilde{Q}=\frac{2\pi Nn_0d^2\omega}{c\hbar\gamma},
\end{aligned}\tag{30}$$

Eq. (29) takes the form

$$\frac{dE_{cm}}{d\zeta} = -\alpha_m E_{cm} + \beta_m E_{sm},$$

$$\frac{dE_{sm}}{d\zeta} = -\alpha_m E_{sm} - \beta_m E_{cm};\ E_{cm}(0) = J_m(\delta),\ \ E_{sm}(0) = 0;$$

$$\alpha_m = \frac{1}{1+(\Omega+m\nu)/\gamma^2},\qquad \beta_m = \frac{\Omega+m\nu/\gamma}{1+\Omega+m\nu^2/\gamma^2}. \tag{31}$$

The solution of Eq. (31) in the case of an optically thin medium, $\zeta_L = \tilde{Q}L \ll 1$, is

$$E_{cm} \approx (1-\alpha_m\zeta_L)J_m(\delta),$$

$$E_{sm} \approx -\beta_m\zeta_L J_m(\delta). \tag{32}$$

It is seen from here that, due to the smallness of $\zeta_L$, $|E_{sm}| \ll |E_{cm}|$. From this relation it follows that the phase shift between the waves at the input and output of an absorbing cell given by $\tan^{-1}(E_{sm}/E_{cm})$ [see Eq. (24)] is also small.

Thus, the amplitude of a field falling on a detector, taking into account Eqs. (24), (31), and (32), is

$$E(t) = E\sum_m J_m(\delta)\{(1-\alpha_m\zeta_L)\cos\,[(\omega+m\nu)t]$$

$$-\beta_m\zeta_L\,\sin\,[(\omega+m\nu)t]\}. \tag{33}$$

The voltage from a detector is proportional to $E^2$ (Eq. (33)) averaged over fast oscillations. In the approximation linear in $\zeta_L$, the signal is

$$I(t) \propto 1 - 2\sum_m \alpha_m J_m^2(\delta)$$

$$+2\sum_{l=1}^{\infty}\sum_{m=-\infty}^{\infty} J_m(\delta)J_{m-l}(\delta)[(1-\alpha_m-\alpha_{m-l})\cos(l\nu t)$$

$$+(\beta_{m-l}-\beta_m)\sin(l\nu t)]. \tag{34}$$

Since according to the Neumann theorem [27]

$$\sum_{\substack{m=-\infty,\\ l\neq 0}}^{\infty} J_m(\delta)J_{m-l}(\delta) = 0,$$

it follows from Eq. (34) that the time-dependent signal at the frequency $l\nu$ is

$$I_l(t) \propto -\sum_m J_m(\delta)J_{m-l}(\delta)[(\alpha_m+\alpha_{m-l})\cos(l\nu t)$$

$$-(\beta_{m-l}-\beta_m)\sin(l\nu t)]. \tag{35}$$

Dual lock-in detection implies the phase shift by $\pi/2$ in one of the channels and adding the phase $\varphi$ in both the channels, which can be manually adjusted [11,18]. Namely, for the first channel we replace $l\nu t \to \varphi$ in Eqs. (35) and $l\nu t \to \varphi+\pi/2$ for the second one. Finally, the spectral dependencies recorded in two channels are

$$K_{1l}(\Omega,\varphi) \propto -\sum_{m=-M+1}^{M-1} J_m(\delta)J_{m-l}(\delta)[(\alpha_m+\alpha_{m-l})$$

$$\times\cos\,\varphi - (\beta_{m-l}-\beta_m)\sin\,\varphi],$$

$$K_{2l}(\Omega,\varphi) \propto \sum_{m=-M+1}^{M-1} J_m(\delta)J_{m-l}(\delta)[(\alpha_m+\alpha_{m-l})\sin\,\varphi$$

$$+(\beta_{m-l}-\beta_m)\cos\,\varphi], \tag{36}$$

where coefficients $\alpha_m$ and $\beta_m$ dependent on the frequency detuning $\Omega$ are given in Eq. (31).

In measurements, it is convenient to adjust the phase $\varphi$ to 0 or $\pi$, in order to maximize the difference between the channels. After such adjustment, the line profile $K_{1l}$ Eq. (36) acts as a simpler equivalent of the line profile Eq. (20). The best results in fitting the obtained profiles to experimental ones can be obtained by means of simultaneous processing spectra recorded in both the channels with the use of the profiles $K_{1l}$ and $K_{2l}$ in Eq. (36).

## 6. Nonlinear mixing of the FM harmonics

The nonlinear resonance interaction of polyharmonical radiation with an absorbing medium must lead to mixing of the FM harmonics that may be essential for optically thick media. Many variants of this physical phenomenon are studied thoroughly in nonlinear optics, but not yet in nonlinear spectroscopy. The aim of a consideration in this section is to clarify how the nonlinear mixing of the FM harmonics in conditions of Lamb dip measurements influences their spectral shape. Let us restrict ourselves by a simple case of small modulation indices $\delta \ll 1$ when only three components of FM radiation with the frequencies $\omega$, $\omega-\nu$, and $\omega+\nu$ are presented. Also we will use the simplified approach similar to those described in Sections 4 and 5. In the framework of this approach, the equations for the density matrix and the representation of a field are

$$\frac{d\rho}{dt} + (\gamma + i\omega_0)\rho = \frac{idE}{\hbar}n,$$

$$\frac{dn}{dt} + \gamma n - \frac{4dE}{\hbar}\mathrm{Re}i\rho = \gamma n_0;$$

$$E(z,t) = E\sum_{n=-1}^{1} E_n(z)\cos\,[(\omega+n\nu)t - k_n z],$$

$$E(0,t) = E\sum_{n=-1}^{1} J_n(\delta)\cos\,[(\omega+n\nu)t]$$

$$\cong E\left\{\cos(\omega t) - \frac{\delta}{2}\cos\,[(\omega-\nu)t] + \frac{\delta}{2}\cos\,[(\omega+\nu)t]\right\}. \tag{37}$$

Here the notations used remain the same as in previous sections. The second of Eq. (37) for the population difference provides nonlinear harmonic's mixing.

We seek the solution of Eq. (37) of the form

$$\rho = \sum_m R_m \exp\{-i[(\omega+m\nu)t - k_m z]\},$$

$$n=\sum_l\{n_{cl}\ \cos\ [l\nu t-(k_l-k_0)z]+n_{sl}\ \sin\ [l\nu t-(k_l-k_0)z]\}. \tag{38}$$

The medium polarization is

$$P=2Nd\mathrm{Re}\rho=\sum_m\{P_{cm}\ \cos\ [(\omega+m\nu)t-k_mz] +P_{sm}\ \sin\ [(\omega+m\nu)t-k_mz]\},$$
$$P_{cm}\equiv\chi'_m=2NdR'_m,\quad P_{sm}\equiv\chi''m=2NdR''_m. \tag{39}$$

The expressions for $P_{cm}$ and $P_{sm}$ following from the solution of Eq. (37) obtained with the accuracy of first nonlinear terms are

$$P_{sm}\approx VP_{sm}^{(0)}+V^3P_{sm}^{(1)},\ P_{cm}\approx VP_{cm}^{(0)},$$
$$P_{sm}^{(0)}=\frac{2Nn_0d\gamma E_m}{\gamma^2+(\Omega+m\nu)^2},\ P_{cm}^{(0)}=-\frac{2Nn_0d(\Omega+m\nu)E_m}{\gamma^2+(\Omega+m\nu)^2},$$
$$m=-1,\ 0,\ 1;$$
$$P_{s-1}^{(1)}=\frac{4Nn_0d\gamma^{-1}}{\gamma^2+(\Omega-\nu)^2}(c_{-1,1}E_{-1}^3+c_{-1,2}E_{-1}E_0^2 +c_{-1,3}E_0^2E_1+c_{-1,4}E_{-1}E_1^2),$$
$$P_{s0}^{(1)}=\frac{4Nn_0dE_0\gamma^{-1}}{\gamma^2+\Omega^2}(c_{0,1}E_{-1}^2+c_{0,2}E_0^2+c_{0,3}E_{-1}E_1+c_{0,4}E_1^2),$$
$$P_{s1}^{(1)}=\frac{4Nn_0d\gamma^{-1}}{\gamma^2+(\Omega+\nu)^2}(c_{1,1}E_1^3+c_{1,2}E_{-1}E_0^2+c_{1,3}E_0^2E_1+c_{1,4}E_{-1}^2E_1). \tag{40}$$

The cubic nonlinearity of $P_{sm}^{(1)}$ in Eq. (40) leads to mixing of the FM harmonics that is analogous to the frequency mixing well known in nonlinear optics. Coefficients $c_{j,l}$ in Eq. (40) dependent on the frequency detuning $\Omega$ are presented in the Appendix. Note that some of coefficients, i.e. $c_{-1,3}$, $c_{0,3}$, and $c_{1,2}$, have the periodic dependence on the wave asynchronism, which is determined by the wave detuning index $\eta$ caused by the difference of real parts of the medium polarization that are linear in field amplitudes:

$$\eta=k_{-1}-2k_0+k_1. \tag{41}$$

The substitution of the following expression for the wave numbers

$$k_m\approx\frac{\omega+m\nu}{c}\left(1+\frac{2\pi}{EE_m}P_{cm}\right) \tag{42}$$

in Eq. (41) gives

$$\eta=-\left(\frac{(\Omega-\nu)/\gamma}{1+(\Omega-\nu)^2/\gamma^2}-\frac{2\Omega/\gamma}{1+\Omega^2/\gamma^2}+\frac{(\Omega+\nu)/\gamma}{1+(\Omega+\nu)^2/\gamma^2}\right)\tilde{Q}, \tag{43}$$

where the factor $\tilde{Q}$ is determined in Eq. (30).

As follows from Eq. (43), the wave detuning $\eta$ depends on $\Omega$. In the case of small $\nu<\gamma$ this dependence is close to the dispersion one, and it causes distortions of a FM harmonic's spectral shape additional to that inherent in coefficients $c_{j,l}(\Omega)$ Eq. (40), which are not related with phases. Note that when the number of harmonics increases, then other wave detuning indices appear, which differ from $\eta$, see Eq. (41).

The wave equations for slow amplitudes taking into account Eq. (40) take the form

$$\frac{dE_m}{d\tilde{\zeta}}=-\frac{E_m}{1+(\Omega+m\nu)^2/\gamma^2}-\kappa\tilde{P}_{sm}^{(1)},$$
$$\tilde{P}_{sm}^{(1)}=\frac{2\pi\omega\gamma^2}{c\tilde{E}Q}P_{sm}^{(1)},\ \kappa=\frac{V^2}{\gamma^2},\ \tilde{\zeta}=\tilde{Q}z,\ m=-1,0,1. \tag{44}$$

The analytical solution of the coupled Eq. (44) can be found in the case of small saturation parameter $\kappa\ll1$ with account of the boundary conditions of Eq. (37) as

$$E_m\approx E_m^{(0)}+\kappa E_m^{(1)},E_{-1}^{(0)}=-\frac{\delta}{2}\exp\left[-\frac{\zeta}{1+(\Omega-\nu)^2/\gamma^2}\right],$$
$$E_0^{(0)}=\exp\left[-\frac{\zeta}{1+\Omega^2/\gamma^2}\right],\quad E_1^{(0)}=\frac{\delta}{2}\exp\left[-\frac{\zeta}{1+(\Omega+\nu)^2/\gamma^2}\right], \tag{45}$$
$$E_m^{(1)}=\int_0^{\zeta}P_{sm}^{(1)}\left[E_m^{(0)}(\zeta)\right]d\zeta.$$

Explicit analytical expressions for $E_m^{(1)}$ in Eq. (45) were determined on the basis of Eq. (40) and (45), but they are somewhat cumbersome to be published.

The spectral line profile for the first FM harmonic detected at the frequency $\nu$ can be found on the basis of

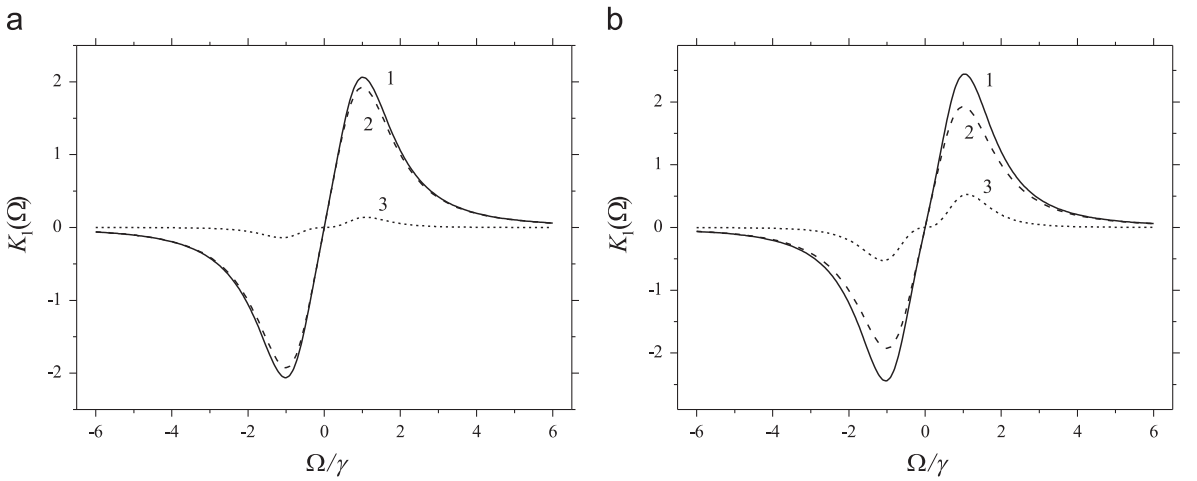


**Fig. 6.** The effect of nonlinear harmonic's mixing on the Lamb dip spectral shape of the first harmonic at the saturation parameter $\kappa=0.04$ (a) and 0.15 (b). Curves 1 represent the complete line profile $K_1(\Omega)$ Eq. (46), curves 2 are related to the profile $K_1^{(0)}$ Eq. (46) without mixing, and curves 3 are residuals or nonlinear part $\kappa K_1^{(1)}$ Eq. (46). $\zeta=0.5$, $\nu=0.7\gamma$, $\delta=0.2$.

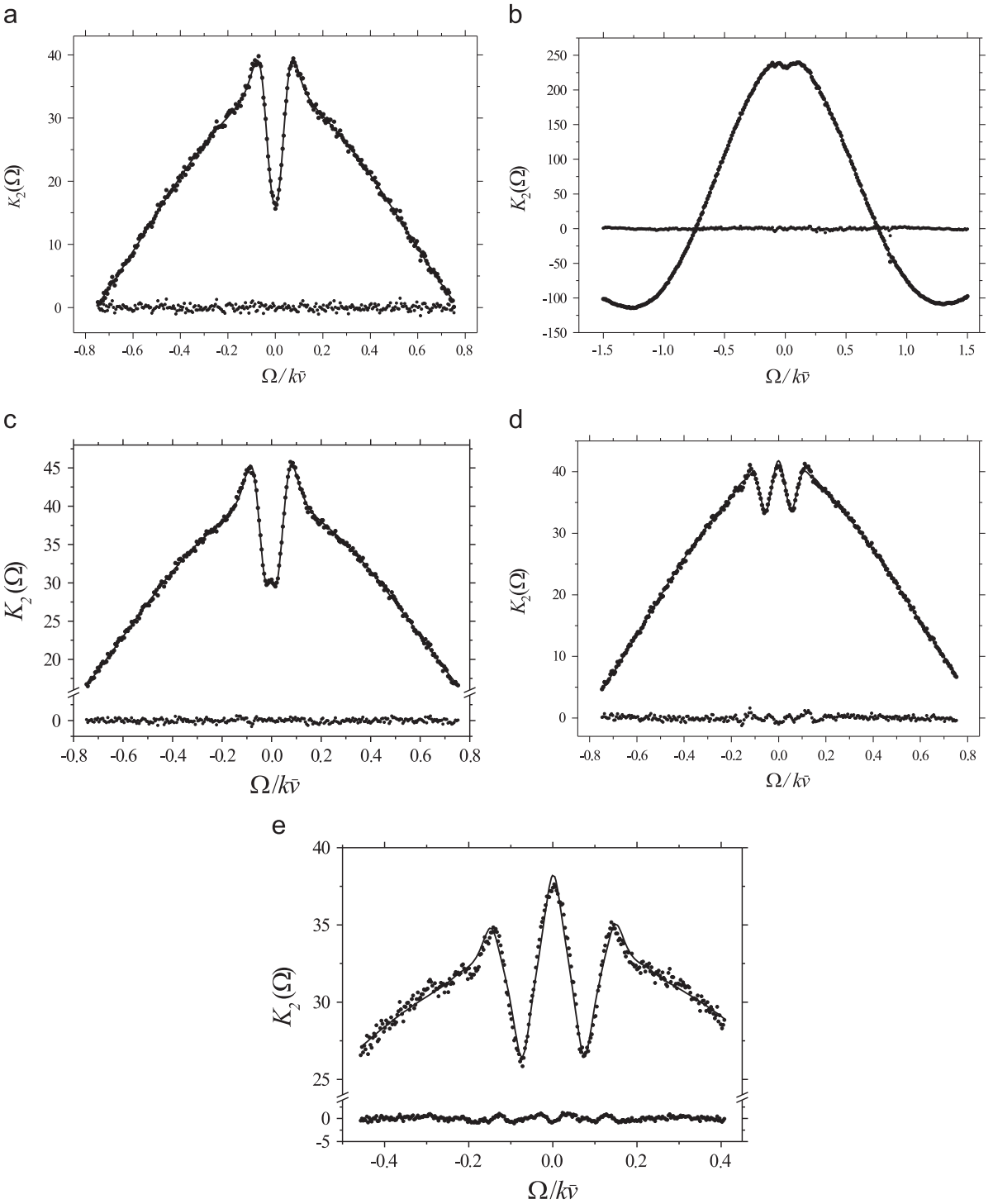


**Fig. 7.** Examples of experimental records of the second harmonic FM nonlinear absorption signals processed with Eq. (20). Fig. 6 a–d displays the 230.538 GHz CO line. The 255.374 OCS line is shown in Fig. 6e. The obtained fitting parameters are: $\gamma/k\bar{v}=0.048$ (a), 0.112 (b), 0.035 (c), 0.032 (d), and 0.028 (e); $\nu/k\bar{v}=0.020$ (a), 0.029 (b), 0.051 (c), 0.106 (d), and 0.147 (e); $\delta=3.01$ (a), 3.16 (b), 1.13 (c), 0.81 (d), and 0.46 (e); $\kappa=0.027$ (a), 0.07 (b), 0.036 (c), 0.024 (d), and 0.063 (e); $\zeta=0.087$ (a), 0.103 (b), 0.181 (c), 0.024 (d), and 0.489 (e). The lower points are residuals.

Eq. (45) and it reads

$$K_1(\Omega) = K_1^{(0)}(\Omega) + \kappa K_1^{(1)}(\Omega);\quad K_1^{(0)}(\Omega) \propto (E_{-1}^{(0)} + E_1^{(0)})E_0^{(0)},$$
$$K_1^{(1)}(\Omega) \propto (E_{-1}^{(1)} + E_1^{(1)})E_0^{(0)} + E_0^{(1)}(E_{-1}^{(0)} + E_1^{(0)}). \quad (46)$$

Line profiles Eq. (46) are plotted in Fig. 6 with the parameters, which values are typical for experiments. As is seen from Fig. 6, the nonlinear mixing of harmonics becomes noticeable at relatively small values of the saturation parameter, starting from $\kappa > 0.04$.

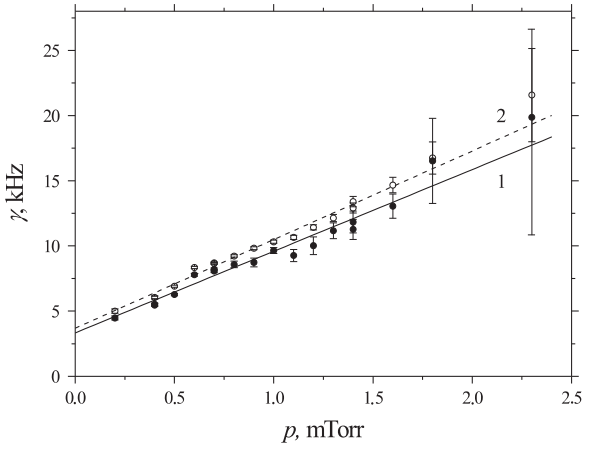


**Fig. 8.** The dependence of the collision half-width on the OCS pressure for the 424.781 GHz line of OCS. The solid line 1 is the linear fit of data obtained in processing with Eq. (20) (black circles), the dashed line 2 is the linear fit of data obtained in processing with Eq. (23) (white circles).

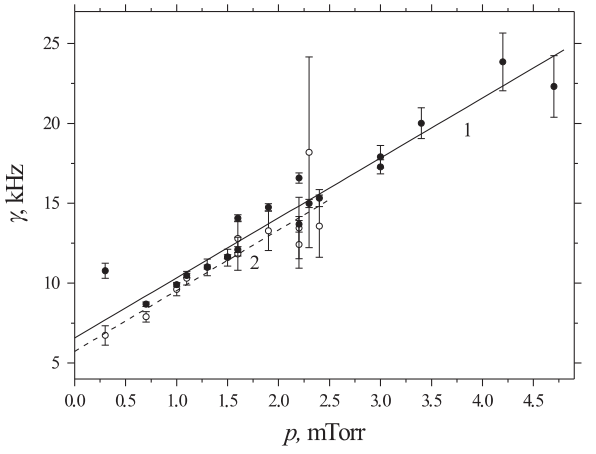


**Fig. 9.** The dependence of the collision half-width on the CO pressure for the 230.538 GHz line of CO. The solid line 1 is the linear fit of data obtained in processing with Eq. (20) (black circles), the dashed line 2 is the linear fit of data obtained in processing with Eq. (36) (white circles).

## 7. Application to experiment

The comparison of theory and experiment was carried out on the example of three spectral lines, the 230.538 GHz line of the CO molecule, the 255.374 and 424.781 GHz lines of the OCS molecule. The detailed description of the experimental setup and conditions of the measurements were previously published [11]. A number of the second FM harmonic nonlinear absorption spectra recorded at various values of a modulation depth, gas pressures, optical thickness, radiation intensity, and modulation frequency have been processed with the line profile Eq. (20) with the use of least squares fitting. The examples are presented in Fig. 7. The curves shown in Fig. 7c, d, and e display the splitting of the Lamb dip recorded with the use of a second harmonic. The splitting takes place at properly high modulation frequencies $\nu > \gamma$ and it evidently follows from the structure of the expression for the line profile Eq. (20). The retrieved fitting parameters $\nu$, $\delta$, and $\zeta_L$ agree with the respective experimentally measured parameters within 10%. Note that the residuals in Fig. 7 have no noticeable trends for all the sets of the used parameters. This fact validates the usage of Eq.(20) in quantitative data processing.

The collision half-width $\gamma$ retrieved from the fitting of line profiles Eqs. (20), (23), and (36) to experimental ones recorded at $\nu < \gamma$ are plotted in Figs. 8 and 9 as a function of gas pressure, respectively for the 424.781 GHz line of OCS and the 230.538 GHz line of CO. The results of a linear approximation for the dependencies $\gamma(p)$ with the weights of separate points, which are inversely proportional to their confidence intervals, are presented in Table 1. From Table 1 it follows that the use of simplified formulas Eqs. (23) and (36) instead of the more general expression Eq. (20) gives acceptable results in retrieving the self-broadening pressure coefficients. Note that the pressure broadening coefficients obtained with the use of simplified formulas Eqs. (23) and (8) give values greater than those retrieved with Eq. (20) by 9% and 12%, respectively. The value of the pressure broadening coefficient obtained for the 424.781 GHz line of OCS matches well with the values 6.3 – 6.8 MHz/Torr measured for closely spaced lines by means of the spectrometer with radio-acoustic detection of absorption linear in radiation intensity [28]. The values of $\gamma$ extrapolated to zero pressure have the same order of magnitude as follows from the above estimations of contributions of the flight effect and the effect of the diffraction molecular scattering. The role of the saturation

**Table 1**
Pressure broadening coefficients retrieved from data processing.

| Line | d$\gamma$ /d$p$, MHz/Torr | $\gamma$ (0), kHz | Fitting line profile |
|---|---|---|---|
| 424.781 GHz OCS | $6.26 \pm 0.35$ | $3.33 \pm 0.26$ | Eq. (20) |
| 424.781 GHz OCS | $6.80 \pm 0.26$ | $3.68 \pm 0.21$ | Eq. (23) |
| 424.781 GHz OCS | $7.00 \pm 0.39$ | $4.42 \pm 0.25$ | 2-nd derivative of Eq. (8) |
| 230.538 GHz CO | $3.75 \pm 0.31$ | $6.57 \pm 0.55$ | Eq. (20) |
| 230.538 GHz CO | $3.79 \pm 0.36$ | $5.73 \pm 0.49$ | Eq. (36) |

effect (power line broadening) in forming $\gamma$ (0) is much less pronounced because of small typical values of the saturation parameter $\kappa \sim 0.02$ obtained from data processing.

## 8. Conclusions

In this paper, the analysis of manifestations of the main physical factors leading to distortion of the Lamb dip spectral shape was carried out. By means of estimations made in Sections 1 and 2 and measurements presented in Figs. 8 and 9, it was shown that the dependence of the collision line width on pressure is linear within the pressure range of $0.2-5$ mTorr, which allows one to obtain pressure broadening coefficients with an inaccuracy $\sim 5\%$. The expressions for Lamb dip shapes recorded with lock-in technique for different FM harmonics were derived. The formula Eq. (20) is valid for arbitrary modulation indices $\delta$ and gives the most complete description of the complicated line profiles of different harmonics of a modulation frequency including line splitting at sufficiently high modulation frequencies $\nu > \gamma$. The increase in $\delta$ leads to essential gain in the recorded signal, but at the same time, the data processing is hampered because of the expansion of the double summation in Eq. (20). For this reason, it is expedient to restrict $\delta < 5$ in measurements. The other resource of simplification of a processing consists in the use of the approximations presented in Eqs. (23), (36), and (8). These simple line profiles have been tested in Section 7 and they provide the retrieved pressure broadening coefficients with systematic errors lesser than 10 percent. In measurements, it is expedient to choose the saturation parameter $\kappa < 0.05$. Otherwise, the recorded spectra undergo distortions due to the power line broadening and the FM harmonic's nonlinear mixing.

## Acknowledgments

This work was financially supported by the Russian Foundation for Basic Research Project No. 13_02_00122).

## Appendix

The coefficients $c_{j,l}$ Eq. (40):

$$c_{-1,1} = -\frac{2\gamma^2}{\gamma^2+(\Omega-\nu)^2},$$

$$c_{-1,2} = -\gamma^2\frac{4\gamma^4+\gamma^2\left(\nu^2-3\nu\Omega+4\Omega^2\right)+\nu\left(\nu^3-3\nu^2\Omega+\nu\Omega^2+\Omega^3\right)}{\left(\gamma^2+\nu^2\right)\left(\gamma^2+\Omega^2\right)\left[\gamma^2+(\Omega-\nu)^2\right]},$$

$$c_{-1,3} = \gamma\left(\begin{array}{l}-\gamma\left(2\gamma^4+\gamma^2(2\Omega-\nu)(\Omega+3\nu)+\nu\left(-\nu^3+\nu^2\Omega+\nu\Omega^2+\Omega^3\right)\right)\cos(\eta z)+\\ \left(-\gamma^4(2\Omega-5\nu)-\nu^2(\Omega^2-\nu^2)\Omega+\gamma^2(2\Omega+\nu)\left(\nu^2+\nu\Omega-\Omega^2\right)\right)\sin(\eta z)\end{array}\right)$$
$$\times\left[\left(\gamma^2+\nu^2\right)\left(\gamma^2+\Omega^2\right)\left(\gamma^2+(\nu+\Omega)^2\right)\right]^{-1},$$

$$c_{-1,4} = -\frac{2\gamma^2}{\gamma^2+(\nu+\Omega)^2},$$

$$c_{0,1} = \frac{\gamma^2}{\gamma^2+\nu^2}\left(\frac{2(\nu\Omega-\gamma^2)}{\gamma^2+\Omega^2}-\frac{\nu\Omega+2\gamma^2}{\gamma^2+(\nu-\Omega)^2}\right),$$

$$c_{0,2} = -\frac{2\gamma^2}{\gamma^2+\Omega^2},$$

$$c_{0,3} = -\left(2\gamma\left(\begin{array}{l}2\gamma(\gamma^2+\nu^2)\left(\gamma^2+\Omega^2\right)\cos(\eta z)+\\ \Omega\left(-2\gamma^4+3\gamma^2\nu^2+\nu^4-(2\gamma^2+\nu^2)\Omega^2\right)\sin(\eta z)\end{array}\right)\right)$$
$$\times\left[\left(\gamma^2+\nu^2\right)\left(\gamma^2+(\Omega-\nu)^2\right)\left(\gamma^2+(\Omega+\nu)^2\right)\right]^{-1},$$

$$c_{0,4} = \frac{\gamma^2}{\gamma^2+\nu^2}\left(\frac{\nu\Omega-2\gamma^2}{\gamma^2+(\Omega+\nu)^2}-\frac{2(\nu\Omega+\gamma^2)}{\gamma^2+\Omega^2}\right),$$

$$c_{1,1} = -\frac{2\gamma^2}{\gamma^2+(\Omega+\nu)^2},$$

$$c_{1,2} = \left(\gamma\left(\begin{array}{l}\gamma\left(\begin{array}{l}-2\gamma^4+\gamma^2(3\nu-\Omega)(\nu+2\Omega)+\\ \nu\left(\nu^3+\nu^2\Omega-\nu\Omega^2+\Omega^3\right)\end{array}\right)\cos(\eta z)-\\ \left(\begin{array}{l}-\nu^4\Omega+\nu^2\Omega^3+\gamma^4(5\nu+2\Omega)+\\ \gamma^2\left(\nu^3-3\nu^2\Omega+\nu\Omega^2+2\Omega^3\right)\end{array}\right)\sin(\eta z)\end{array}\right)\right)$$

$$\times\left[\left(\gamma^2+\nu^2\right)\left(\gamma^2+(\Omega-\nu)^2\right)\left(\gamma^2+\Omega^2\right)\right]^{-1},$$

$$c_{1,3}=-\frac{\gamma^2\left(4\gamma^4+\nu(\Omega+\nu)\left(\nu^2+2\nu\Omega-\Omega^2\right)+\gamma^2\left(\nu^2+3\nu\Omega+4\Omega^2\right)\right)}{\left(\gamma^2+\nu^2\right)\left(\gamma^2+\Omega^2\right)\left(\gamma^2+(\Omega+\nu)^2\right)},$$

$$c_{1,4}=-\frac{2\gamma^2}{\gamma^2+(\Omega-\nu)^2}.$$

## References


[1] Letokhov VS, Chebotayev VP. Nonlinear laser spectroscopy. Berlin/Heidelberg/New York: Springer-Verlag; 1977. [Letokhov VS, Chebotayev VP. Foundations of nonlinear laser spectroscopy. Moscow: Mir; 1975].

[2] Cazzoli G, Puzzarini C, Harding ME, Gauss J. The hyperfine structure in the rotation spectra of water: Lamb-dip technique and quantum-chemical calculations. Chem Phys Lett 2009;473:21–5.

[3] Karplus R, Schwinger IA. Note on saturation in microwave spectroscopy. Phys Rev 1948;73:1020–6.

[4] Rautian SG, Shalagin AM. Saturation effects for long-lived systems in spatially bounded fields. J Exp Theor Phys 1970;31:518–23. [Zh. eksp. teor. fiz. 1970; 58: 962 – 74].

[5] Bagayev SN, Chebotayev VP. Laser frequency standards. Uspekhi Fiz Nauk 1986;148:143–78.

[6] Bagayev SN, Baklanov EV, Chebotayev VP. Measurement of elastic scattering crosssections in a gas by laser spectroscopy methods. ZhETF Pis Red 1972;16:15–8. [Pisma v Zh. eksp. teor. fiz. 1972; 16: 15 – 8].

[7] Vasilenko LS, Kochanov VP, Chebotayev VP. Opt Commun 1977;20:409–11.

[8] Kochanov VP, Rautian SG, Shalagin AM. Broadening of nonlinear resonances by velocity-changing collisions. J Exp Theor Phys 1977;45:714–22. [Zh. eksp. teor. fiz. 1977; 72: 1358 – 74].

[9] Bennett Jr. WR. Hole burning effects in a He–Ne maser. Phys Rev 1962;126:580–93.

[10] Lamb WE. Theory of optical maser. Phys. Rev 1964;134:1429–50.

[11] Golubyatnikov GYu, Belov SP, Leonov II, Andrianov AF, Zinchenko II, Lapinov AV, et al. Precision sub-Doppler millimeter and submillimeter Lamb-dip spectrometer. Radiophys Quantum Electron 2014;56:599–609 [IzvestiyaVuzov, Radiofizika 2013; 56: 666–677].

[12] Karplus R. Frequency modulation in microwave spectroscopy. Phys Rev 1948;73:1027–34.

[13] Wahlquist H. Modulation broadening of unsaturated Lorentzian lines. J Chem Phys 1961;35:1708–10.

[14] Arndt R. Analytical line shapes for Lorentzian signals broadened by modulation. J Appl Phys 1965;36:2522–4.

[15] Reid J, Labrie D. Second-harmonic detection with tunable diode lasers – comparison of experiment and theory. Appl Phys B 1981;26:203–10.

[16] Bjorklund GC, Levenson MD, Lenth W, Ortiz C. Frequency modulation (FM) spectroscopy. Theory of lineshapes and signal-to-noise analysis. Appl Phys B 1983;32:145–52.

[17] Cazzoli G, Dore L. Lineshape measurements of rotational lines in the millimeter-wave region by second harmonic detection. J Mol Spectrosc 1990;141:49–58.

[18] North SW, Zheng XS, Fei R, Hall GE. Line shape analysis of Doppler broadened frequency-modulated line spectra. J Chem Phys 1996;104:2129–35.

[19] Vaks VL, Khodos VV, Spivak EV. A nonstationary microwave spectrometer. Rev Sci Instrum 1999;70:3447–52.

[20] Puzzarini C, Dore L, Cazzoli G. A comparison of lineshape models in the analysis of modulated and natural rotational line profiles: application to the pressure broadening of OCS and CO. J Mol Spectrosc 2002;216:428–36.

[21] Dore L. Using fast Fourier transform to compute the line shape of frequency-modulated spectral profiles. J Mol Spectrosc 2003;221:93–8.

[22] De Tommasi E, Castrillo A, Casa G, Gianfrani L. An efficient approximation for a wavelength-modulated 2nd harmonic lineshape from a Voigt absorption profile. J Quant Spectrosc Radiat Transf 2008;109:168–75.

[23] Rautian SG, Smirnov GI, Shalagin AM. Nonlinear resonances in spectra of atoms and molecules. Novosibirsk: Nauka SB; 1979.

[24] Rautian SG, Shalagin AM. Kinetic problems of non-linear spectroscopy. Amsterdam: North-Holland; 1991.

[25] Kochanov VP. Manifestations of small-angle molecular scattering in spectral line profiles. J Exp Theor Phys 2014;118:335–50. [Zh. Eksp. Teor. Fiz. 2014; 145: 387–404].

[26] Dicke RH. The effect of collisions upon the Doppler width of spectral lines. Phys Rev 1953;89:472–3.

[27] Abramowitz M, Stegan IA, editors. Handbook of mathematical functions. NBS Applied mathematics, series 55; 1964.

[28] Koshelev MA, Tretyakov MYu, Rohart F, Bouanich J-P. Speed dependence of collisional relaxation in ground vibrational state of OCS: rotational behaviour. J Chem Phys 2012;136:124316.